Engineering Structures 87 (2015) 21–31

Contents lists available at ScienceDirect

Engineering Structures

journal homepage: www.elsevier.com/locate/engstruct

A theoretical formulation for the stress analysis of multi-segmented spherical shells for high-volume liquid containment

Alphose Zingoni *, Batho Mokhothu, Nosakhare Enoma

Department of Civil Engineering, University of Cape Town, Rondebosch, 7701 Cape Town, South Africa

ARTICLE INFO

Article history:
Received 1 October 2014
Revised 31 December 2014
Accepted 2 January 2015

Keywords:
Shell of revolution
Shell analysis
Containment shell
Discontinuity stresses
Storage vessel
Membrane theory of shells
Bending theory of shells

ABSTRACT

A linear-elastic theoretical formulation is presented for the complete determination of the state of stress in large thin-walled liquid-filled vessels in the form of multi-segmented spherical shells. The transfer of membrane forces between adjacent shell segments is such that only vertical equilibrium of stress resultants needs to be preserved. The edge effect in the vicinity of the shell junctions is quantified on the basis of an approximate but accurate bending theory for spherical shells. The effectiveness of the developed formulation is demonstrated by consideration of a numerical example. Agreement with the results of finite-element modelling is excellent, showing that the presented theoretical formulation is a reliable, computationally efficient and accurate means of obtaining stresses in large multi-segmented spherical vessels.

1. Introduction

Thin synclastic shells of revolution find widespread application in the storage of liquids [1], on account of the structural efficiency of shells of double curvature, which allows very thin shells to resist relatively large hydrostatic pressures without rupture. Containment shells of double curvature come in a variety of shapes, from spherical, ellipsoidal, toroidal and other basic mathematical profiles, to combinations of these profiles, giving an almost limitless range of possibilities. The construction may be in thin metal, or in prestressed concrete. However, where compressive stresses exist, these structures are vulnerable to local buckling on account of the thin-ness of the shell, particularly in the case of metal construction. The thickness of the shell may be enhanced in such zones to counter any tendencies for local buckling, or stiffeners may be added to the basic shell.

Fig. 1 shows a novel form of construction for high-capacity liquid-storage vessels. The construction consists of an assembly of spherical shell segments of different radii, whose centres of curvatures all lie on the axis of revolution of the vessel taken as a whole. Thus the segments are axisymmetric in shape, where the uppermost segment is actually a cap, and successive lower segments are typically spherical frusta. Let us denote the various shells regions or segments, from top to bottom, by S1, S2, S3 and so forth. The junctions between these shell segments are denoted by J1, J2, J3 and so forth. The radii of shell S1, S2, S3, etc. are denoted by a_1, a_2, a_3 and so forth. As is usual for shells of revolution, the angular coordinate ϕ (which is the angle between the normal to the shell midsurface at any given point, and the axis of revolution of the shell assembly) is used to define the position of any point on the shell. For the shell cap S1 (uppermost portion of the assembly), the angular coordinate of the edge of the cap is denoted by ϕ_{10}. For all other segments Si ($i = 2, 3, 4$, etc.) below this, the upper and lower edges of segment Si are defined by the coordinates ϕ_{i1} and ϕ_{i2} respectively.

Starting from the central segment (S4 in our illustration), the addition of segments S3, S2 and S1, with slope enhancements of $(\phi_{32} - \phi_{41})$, $(\phi_{22} - \phi_{31})$ and $(\phi_{10} - \phi_{21})$ at junctions J3, J2 and J1 respectively, adds height and additional storage capacity to the basic spherical vessel of radius a_4. Similar enhancements in capacity are also achieved by the addition of segments S5, S6 and S7 in the lower part of the vessel. The overall result is a spherical assembly of relatively large storage capacity. It is interesting to note that if this was a pressure vessel, to achieve the same storage capacity while keeping the vessel of constant radius would require a sphere of radius bigger than a_4, which would attract higher shell stresses (these are proportional to the radius), but in the present case of liquid containment, the stress-reducing benefit of radius limitation

* Corresponding author. Tel.: +27 (21) 650 2601; fax: +27 (21) 650 3293.
E-mail address: alphose.zingoni@uct.ac.za (A. Zingoni).

http://dx.doi.org/10.1016/j.engstruct.2015.01.002
0141-0296/

through segmental construction is offset by the higher hydrostatic pressures associated with the taller segmented vessel.

The slope and curvature discontinuities at the shell junctions attract bending disturbances [2–5], but the inward pointing kinks in the profile could have the effect of stiffening the shell response there, resulting in a beneficial lowering of hoop stresses. From an aesthetics point of view, the "lobed" or segmented geometry of the storage vessel has a pleasing appearance, which might favour the adoption of this type of vessel in locations where appearance is a major consideration.

The membrane theory of axisymmetrically loaded shells of revolution is quite appropriate for the calculation of the linear elastic response of the shell under internal hydrostatic pressure. This theory assumes there is no bending in the shell. However, and as is well-known [2–5], the membrane theory becomes inadequate in the vicinity of geometric discontinuities of the type J1, J2, J3, etc., and the more comprehensive bending theory of shells must be invoked.

A useful approach is to regard the membrane solution (for the applied surface loading on the shell) as an approximate particular solution of the differential equations describing the behaviour of the shell, and a bending correction (system of axisymmetric bending moments and shearing forces applied along the shell edge) as the homogeneous solution [2–5]; the net response of the shell is then obtained as the sum of the membrane solution and the bending correction (or edge effect). Several bending theories of varying degrees of complexity have been proposed for determining the state of stress in shells of revolution [2,3]. However, it is important to select an approach that is amenable to practical computations, and that is sufficiently accurate.

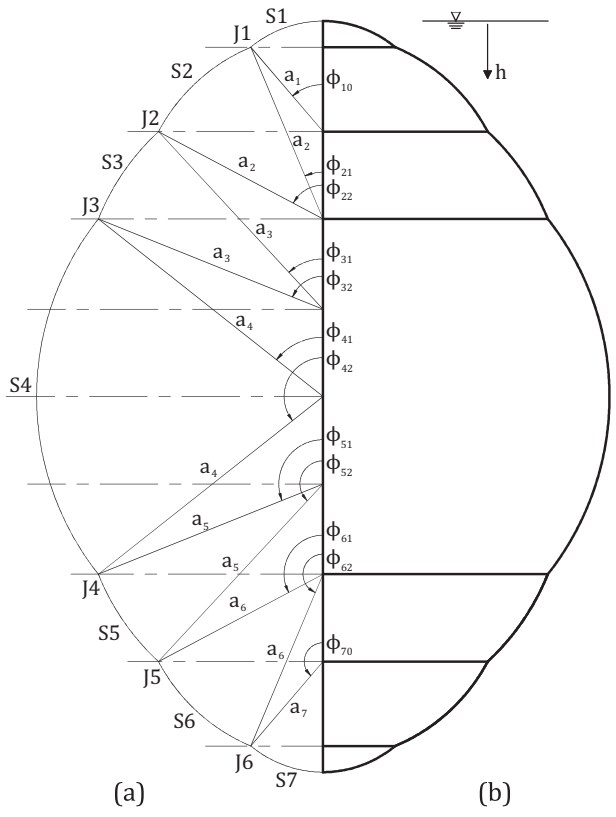

Fig. 1. Multi-segmented spherical vessel: (a) shell segments, junctions and corresponding geometric parameters; (b) external appearance of the vessel.

Not many analytical studies on the stress and deformation behaviour of liquid-containment shells of revolution are being reported in the literature nowadays, largely due to the fact that the Finite Element Method (FEM) has become the preferred method for investigating shell behaviour [6–8], owing to its versatility in handling irregular features of the structure, and in modelling non-linear behaviour. However, the analytical approach can still be extremely useful in those instances where the behaviour of the shell is essentially linear, and convenient mathematical solutions of the differential equations (governing shell behaviour) exist. The analytical approach, where possible, has the advantage of providing stress information without the need for potentially expensive numerical modelling, and shedding deeper insights into the behaviour of the shell simply by studying the form of the mathematical solutions. Once the analytical results are there, they may be treated as formulae, ready to be directly applied to other similar problems. Analytical solutions are also vital in checking FEM results.

Where smoothness conditions prevail, the membrane solution on its own can be a very useful tool for exploring the state of stress in liquid containment vessels in the form of arbitrary shells of revolution [9], or unusual shapes such as the triaxial ellipsoid [10]. However, where the shell geometry features discontinuities, such as sudden changes in shell thickness [11,12], a more general formulation accounting for bending effects clearly has to be employed.

Looking at the more recent literature on liquid-containment vessels, we find that cylindrical steel tanks have been studied the most. Wind-induced buckling of cylindrical tanks has received a considerable amount of attention [13,14]; such tanks are particularly vulnerable when they are empty (the presence of liquid tends to stabilise the shell against the effects of the wind). Tanks that are in close proximity of each other attract additional problems of wind interference, a phenomenon that has been the subject of some very recent studies [15,16]. Other studies have considered the response of liquid-storage cylindrical tanks to seismic excitation [17–19]. The collapse behaviour of large cylindrical steel tanks has also received attention [20], to provide a better understanding of ultimate limit-state design of such vessels. Much of the research on metal containment shells has now been codified [21,22].

At wastewater treatment works, egg-shaped digesters (with their smoothly varying geometry) offer a solution that is superior to cylindrical tanks and more conducive to the efficient mixing of sludge. The stresses and deformations in egg-shaped vessels have been investigated on the basis of the membrane theory and a simplified bending theory for shells of revolution [23,24]. A novel form of sludge digester in the form of a parabolic ogival shell has also been proposed [25], and investigated on the basis of a membrane-theory formulation, leading to some interesting insights on the behaviour of this shell form, and a set of design recommendations.

After cylindrical steel tanks, conical steel tanks come second in having been studied the most, on account of their ease of fabrication. Most previous studies on conical tanks have either sought to understand stability behaviour [26], or to develop appropriate design procedures [27]. Other studies have concentrated on understanding shell-junction effects [28,29], or the effects of external pressure [30]. The stability of vessels in the form of conical-cylindrical assemblies is a subject that has also received a considerable amount of attention [31,32].

For horizontal tanks, deviations from the normal cylindrical shape have been shown to offer enhanced structural efficiencies in comparison with conventional profiles [33]. Another class of vessel that has been studied, albeit to a lesser extent, is that of toroidal tanks [34], which find application for the storage of liquefied petroleum gas (LPG), among others. Depending on the type of cross-section chosen for the toroid, the stress distribution and

stability behaviour can differ quite markedly from one toroidal form to another. For a general appreciation of the great diversity of shell forms that are available for liquid-storage purposes, the reader is referred to the excellent survey of Tooth [1]. A general review of shell buckling has also been conducted by Teng [35].

In this paper, we will focus on large liquid containment shell structures of the type depicted in Fig. 1, and develop an analytical formulation for the complete stress determination in such vessels. The considerations only apply to the behaviour of the shell assembly within the linear elastic range. This is justified since linear elastic response is often used as a basis of preliminary design and compliance with serviceability requirements, with non-linear simulations being reserved for investigating large displacements, buckling and collapse behaviour of the shell.

It is worth pointing out that the presented general solution strategy for liquid containment vessels of the type in question is also applicable for other multi-segmented shell structures such as roof domes, the only difference being the loading to which the shells are subjected.

2. Loading preliminaries

Assuming the vessel is completely filled with liquid of weight γ per unit volume, the hydrostatic pressure p_r on the inside surface of the shell at a depth h from the top (refer to Fig. 1) is given by

$$p_r = \gamma h \tag{1}$$

Let us denote by $h_i(\phi)$ the depth of liquid at the coordinate ϕ of shell S*i*. For the very top shell (S1), which has a radius a_1, the depth of liquid at any given point is given by

$$h_1(\phi) = a_1(1-\cos\phi) \quad [0 \leqslant \phi \leqslant \phi_{10}] \tag{2a}$$

At $\phi = \phi_{10}$, we have

$$h_{10} = a_1(1-\cos\phi_{10}) \tag{2b}$$

For shell S2, which has a radius of a_2, the depth of liquid at the coordinate ϕ of this shell (notice that each shell has its own range of ϕ values) is given by

$$h_2(\phi) = h_{10} + a_2(\cos\phi_{21} - \cos\phi) \quad [\phi_{21} \leqslant \phi \leqslant \phi_{22}] \tag{3a}$$

At $\phi = \phi_{22}$, we have

$$h_{22} = h_{10} + a_2(\cos\phi_{21} - \cos\phi_{22}) \tag{3b}$$

For shell S3, which has a radius of a_3, the depth of liquid at the coordinate ϕ of this shell is given by

$$h_3(\phi) = h_{22} + a_3(\cos\phi_{31} - \cos\phi) \quad [\phi_{31} \leqslant \phi \leqslant \phi_{32}] \tag{4a}$$

At $\phi = \phi_{32}$, we have

$$h_{32} = h_{22} + a_3(\cos\phi_{31} - \cos\phi_{32}) \tag{4b}$$

In general, for shell S*i* ($i > 2$), which has a radius of a_i, the depth of liquid at the coordinate ϕ of this shell is given by

$$h_i(\phi) = h_{(i-1)2} + a_i(\cos\phi_{i1} - \cos\phi) \quad [\phi_{i1} \leqslant \phi \leqslant \phi_{i2}] \tag{5a}$$

At $\phi = \phi_{i2}$, we have

$$h_{i2} = h_{(i-1)2} + a_i(\cos\phi_{i1} - \cos\phi_{i2}) \tag{5b}$$

A more general way of expressing the results for all shell regions S*i*, where this time $i = 1, 2, \ldots, I$ (I being the total number of shell segments, e.g. $I = 7$ for the vessel in Fig. 1), is achieved by writing $h_i(\phi)$ as follows:

$$h_i(\phi) = k_i - a_i\cos\phi \tag{6}$$

where the parameter k_i is a constant defined differently for the various regions as follows:

$$\text{for } i = 1: \quad k_i = k_1 = a_1 \tag{7a}$$

$$\text{for } i = 2: \quad k_i = k_2 = h_{10} + a_2\cos\phi_{21} \tag{7b}$$

$$\text{for } 2 < i < I: \quad k_i = h_{(i-1)2} + a_i\cos\phi_{i1} \tag{7c}$$

$$\text{for } i = I: \quad k_i = k_I = h_{(I-1)2} + a_I\cos\phi_{I0} \tag{7d}$$

Substituting the above generalised expression for $h_i(\phi)$ in Eq. (1), the hydrostatic pressure p_r at any given point of any given shell S*i* ($i = 1, 2, \ldots, I$) becomes

$$p_r(\phi) = \gamma h_i(\phi) = \gamma k_i - \gamma a_i\cos\phi \tag{8}$$

3. Membrane stress resultants

For axisymmetrically loaded shells of revolution, the meridional and hoop membrane stress resultants (forces per unit length of the shell, considered positive when tensile) are given by the well-known general solutions [3–5]

$$N_\phi = \frac{1}{r_2\sin^2\phi}\int r_1 r_2(p_r\cos\phi - p_\phi\sin\phi)\sin\phi d\phi + A \tag{9}$$

$$\frac{N_\phi}{r_1} + \frac{N_\theta}{r_2} = p_r \tag{10}$$

where r_1 and r_2 are principal radii of curvature of the shell midsurface at the point in question, p_r and p_ϕ are loading components (forces per unit area of the shell surface) normal to the shell midsurface and tangential to the shell meridian respectively, and A is a constant of integration.

For a spherical shell, $r_1 = r_2 = a$ (radius of the spherical shell). If hydrostatic pressure is the only loading applied, then $p_\phi = 0$. Eq. (9) simplifies to

$$N_\phi = \frac{1}{a_i\sin^2\phi}\left[a_i^2\int p_r\cos\phi\sin\phi d\phi + B_i\right] \tag{11}$$

for every spherical shell region S*i* of the vessel in Fig. 1. Substituting the expression for p_r (Eq. (8)) into this equation and evaluating the integral, we obtain

$$N_\phi = \frac{1}{6}\frac{\gamma a_i^2}{\sin^2\phi}\left(2\cos^3\phi - 3\frac{k_i}{a_i}\cos^2\phi + C_i\right) \tag{12}$$

where the constant of integration C_i has to be evaluated from a suitable boundary condition.

The constant of integration C_i for the end shells (shell S1 and shell SI) may be evaluated from the finiteness condition for N_ϕ in these regions. For shell S1 (top of the vessel),

$$N_\phi^{(1)} = \frac{1}{6}\frac{\gamma a_1^2}{\sin^2\phi}(2\cos^3\phi - 3\cos^2\phi + C_1) \tag{13a}$$

(the notation $N_\phi^{(1)}$ denoting N_ϕ for shell S1). The finiteness condition for N_ϕ at $\phi = 0$ (apex of the vessel) gives $C_1 = 1$, so that

$$N_\phi^{(1)} = \frac{\gamma a_1^2}{6}\left(\frac{1-\cos\phi}{1+\cos\phi}\right)(1+2\cos\phi) \tag{13b}$$

The hoop stress resultant follows from Eq. (10):

$$N_\theta^{(1)} = \frac{\gamma a_1^2}{6}\left(\frac{1-\cos\phi}{1+\cos\phi}\right)(5+4\cos\phi) \tag{13c}$$

These are well-known results for spherical tanks [3,5].

For shell SI (bottom of the vessel), with the parameter k_I as defined by expression (7d), Eq. (12) may be written as

$$N_\phi^{(I)} = \frac{1}{6}\frac{\gamma a_I^2}{\sin^2\phi}\left(2\cos^3\phi - 3\frac{k_I}{a_I}\cos^2\phi + C_I\right) \tag{14a}$$

The finiteness condition for N_ϕ at $\phi = \pi$ (the zenith of the vessel) gives

$$C_I = 2 + 3\frac{k_I}{a_I} \tag{14b}$$

The meridional and hoop stress resultants in this part of the vessel (shell SI) are therefore:

$$N_\phi^{(I)} = \frac{1}{6}\frac{\gamma a_I^2}{\sin^2\phi}\left(2 + 3\frac{k_I}{a_I}\sin^2\phi + 2\cos^3\phi\right) \tag{14c}$$

$$N_\theta^{(I)} = \frac{1}{6}\gamma a_I^2\left\{3\frac{k_I}{a_I} + \left(\frac{2}{1-\cos\phi}\right)(2\cos^2\phi - 2\cos\phi - 1)\right\} \tag{14d}$$

Consider the interface of shell S1 and shell S2 (that is, junction J1 in Fig. 1). For shell S1, the value of N_ϕ at junction J1 (where ϕ for this shell is equal to ϕ_{10}) is given by:

$$\left(N_\phi^{(1)}\right)_{\phi=\phi_{10}} = N_{\phi 1}^{(1)} = \frac{1}{6}\frac{\gamma a_1^2}{\sin^2\phi_{10}}(1 - 3\cos^2\phi_{10} + 2\cos^3\phi_{10}) \tag{15}$$

For shell S2, the value of N_ϕ at junction J1 (where ϕ for this shell is equal to ϕ_{21}) is given by:

$$\left(N_\phi^{(2)}\right)_{\phi=\phi_{21}} = N_{\phi 1}^{(2)} = \frac{1}{6}\frac{\gamma a_2^2}{\sin^2\phi_{21}}\left(2\cos^3\phi_{21} - 3\frac{k_2}{a_2}\cos^2\phi_{21} + C_2\right) \tag{16}$$

Fig. 2 shows the forces acting upon the portion of the vessel above a horizontal cross-section *Y–Y* located at an arbitrary depth *y* below the apex of the vessel and within the domain of shell S2. We will refer to such a single-edged portion of the vessel as a *cap*. Let the radius of the circular edge of the cap be denoted by *R*. The force $W(y)$ represents the vertical resultant of the hydrostatic pressure acting over the entire surface of the cap. Treating the cap as a free-body diagram, we see that $W(y)$ is balanced by the vertical component of the stress resultants $N_\phi(y)$ acting along the circular edge of the cap. We may therefore write:

$$W(y) = N_\phi(y)\sin\phi(2\pi R) \tag{17}$$

Let the vertical resultant on the portion of the vessel above junction J1 (that is, on shell S1) be denoted by W_o. Let the value of *R* at junction J1 be denoted by R_1. At junction J1, just within shell S1, we may write

$$W_o = N_{\phi 1}^{(1)}\sin\phi_{10}(2\pi R_1) \tag{18a}$$

and just within shell *S2*, we may write

$$W_o = N_{\phi 1}^{(2)}\sin\phi_{21}(2\pi R_1) \tag{18b}$$

From these two expressions for W_o, we deduce that

$$N_{\phi 1}^{(2)} = \left(\frac{\sin\phi_{10}}{\sin\phi_{21}}\right)N_{\phi 1}^{(1)} \tag{19a}$$

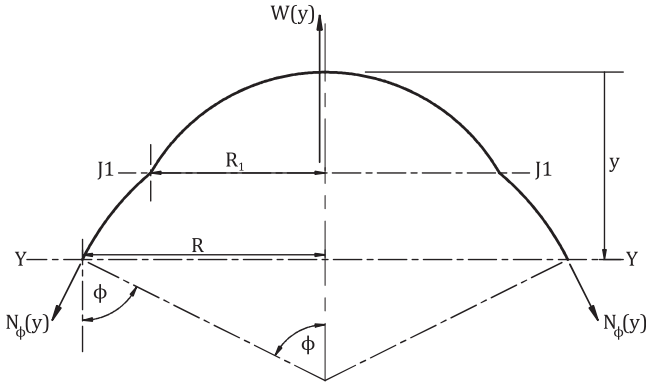

Fig. 2. Forces acting upon a spherical cap above a horizontal section *Y–Y*.

which is the condition of vertical equilibrium at junction J1. Substituting the expressions for $N_{\phi 1}^{(1)}$ and $N_{\phi 1}^{(2)}$ (Eqs. (15) and (16)) into Eq. (19a), we obtain

$$\frac{1}{6}\frac{\gamma a_2^2}{\sin^2\phi_{21}}\left(2\cos^3\phi_{21} - 3\frac{k_2}{a_2}\cos^2\phi_{21} + C_2\right) = \left(\frac{\sin\phi_{10}}{\sin\phi_{21}}\right)\frac{1}{6}\frac{\gamma a_1^2}{\sin^2\phi_{10}}(1 - 3\cos^2\phi_{10} + 2\cos^3\phi_{10}) \tag{19b}$$

giving the solution

$$C_2 = \frac{a_1^2}{a_2^2}\left(\frac{\sin\phi_{21}}{\sin\phi_{10}}\right)(1 - 3\cos^2\phi_{10} + 2\cos^3\phi_{10}) - 2\cos^3\phi_{21} + 3\frac{k_2}{a_2}\cos^2\phi_{21} \tag{20}$$

Using this result in Eq. (12) (to eliminate C_i for $i = 2$), we can write N_ϕ for shell S2 in explicit form, and in turn using the ensuing expression for N_ϕ in Eq. (10), we also obtain the hoop stress resultant N_θ in explicit form. The results are:

$$N_\phi^{(2)} = \frac{1}{6}\frac{\gamma a_2^2}{\sin^2\phi}\left\{\left(2\cos^3\phi - 3\frac{k_2}{a_2}\cos^2\phi\right) - \left(2\cos^3\phi_{21} - 3\frac{k_2}{a_2}\cos^2\phi_{21}\right) + \frac{a_1^2}{a_2^2}\left(\frac{\sin\phi_{21}}{\sin\phi_{10}}\right)(1 - 3\cos^2\phi_{10} + 2\cos^3\phi_{10})\right\} \tag{21a}$$

$$N_\theta^{(2)} = a_2 p_r - N_\phi^{(2)} = \frac{\gamma a_2^2}{6}\left[6\left(\frac{k_2}{a_2} - \cos\phi\right) - \frac{1}{\sin^2\phi}\left\{\left(2\cos^3\phi - 3\frac{k_2}{a_2}\cos^2\phi\right) - \left(2\cos^3\phi_{21} - 3\frac{k_2}{a_2}\cos^2\phi_{21}\right) + \frac{a_1^2}{a_2^2}\left(\frac{\sin\phi_{21}}{\sin\phi_{10}}\right)(1 - 3\cos^2\phi_{10} + 2\cos^3\phi_{10})\right\}\right] \tag{21b}$$

where from Eqs. (7b) and (2b), k_2 has the explicit form

$$k_2 = h_{10} + a_2\cos\phi_{21} = a_1(1 - \cos\phi_{10}) + a_2\cos\phi_{21} \tag{22}$$

For any subsequent shell S*i* ($i > 2$), the C_i in Eq. (12) is obtained from

$$N_{\phi(i-1)}^{(i)} = \left(\frac{\sin\phi_{(i-1)2}}{\sin\phi_{i1}}\right)N_{\phi(i-1)}^{(i-1)} \tag{23}$$

which is the condition of vertical equilibrium at junction J$(i-1)$, noting that the $(i-1)$ in the subscript for N_ϕ refers to junction J$(i-1)$ between shell S$(i-1)$ and shell S*i*. Expanding the N_ϕ terms in Eq. (23) on the basis of Eq. (12), and re-arranging, we obtain

$$C_i = \frac{a_{i-1}^2}{a_i^2}\left(\frac{\sin\phi_{i1}}{\sin\phi_{(i-1)2}}\right)\left(2\cos^3\phi_{(i-1)2} - 3\frac{k_{i-1}}{a_{i-1}}\cos^2\phi_{(i-1)2} + C_{i-1}\right) - \left(2\cos^3\phi_{i1} - 3\frac{k_i}{a_i}\cos^2\phi_{i1}\right) \tag{24}$$

where C_{i-1} is known from the preceding step. With C_i now known, the stress resultants $N_\phi^{(i)}$ and $N_\theta^{(i)}$ for shell S*i* (where $i = 3, 4, \ldots, (I-1)$) then follow:

$$N_\phi^{(i)} = \frac{1}{6}\frac{\gamma a_i^2}{\sin^2\phi}\left\{\left(2\cos^3\phi - 3\frac{k_i}{a_i}\cos^2\phi\right) - \left(2\cos^3\phi_{i1} - 3\frac{k_i}{a_i}\cos^2\phi_{i1}\right) + \frac{a_{i-1}^2}{a_i^2}\left(\frac{\sin\phi_{i1}}{\sin\phi_{(i-1)2}}\right)\left(2\cos^3\phi_{(i-1)2} - 3\frac{k_{i-1}}{a_{i-1}}\cos^2\phi_{(i-1)2} + C_{i-1}\right)\right\} \tag{25a}$$

$$N_\theta^{(i)} = \frac{\gamma a_i^2}{6}\left[6\left(\frac{k_i}{a_i} - \cos\phi\right) - \frac{1}{\sin^2\phi}\left\{\left(2\cos^3\phi - 3\frac{k_i}{a_i}\cos^2\phi\right) - \left(2\cos^3\phi_{i1} - 3\frac{k_i}{a_i}\cos^2\phi_{i1}\right) + \frac{a_{i-1}^2}{a_i^2}\left(\frac{\sin\phi_{i1}}{\sin\phi_{(i-1)2}}\right)\left(2\cos^3\phi_{(i-1)2} - 3\frac{k_{i-1}}{a_{i-1}}\cos^2\phi_{(i-1)2} + C_{i-1}\right)\right\}\right] \tag{25b}$$

Note that the above expressions are only valid for regions of the shell above the level of the supports. For regions below the level of the supports, the constants have to be evaluated successively from the bottom upwards (since C_I is known) until we get to the supports.

In the process of calculating the edge effects around the junction locations (which we will deal with later), the horizontal resultant of the membrane meridional stress resultants at a junction will be required. Consider junction J*i* between shell S*i* and shell S$(i+1)$. The horizontal resultant H_i^m at this junction (the superscript m denoting association with the membrane solution) is simply given by the difference between the horizontal components of the membrane meridional stress resultants at the edges of the two shells:

$$H_i^m = N_{\phi i}^{(i)} \cos\phi_{i2} - N_{\phi i}^{(i+1)} \cos\phi_{(i+1)1} = \frac{1}{6}\frac{\gamma a_i^2}{\sin^2\phi_{i2}} \left(2\cos^3\phi_{i2} - 3\frac{k_i}{a_i}\cos^2\phi_{i2} + C_i\right)\cos\phi_{i2} - \frac{1}{6}\frac{\gamma a_{i+1}^2}{\sin^2\phi_{(i+1)1}} \left(2\cos^3\phi_{(i+1)1} - 3\frac{k_{i+1}}{a_{i+1}}\cos^2\phi_{(i+1)1} + C_{i+1}\right)\cos\phi_{(i+1)1} \quad (26)$$

4. Membrane deformations

Relevant to the evaluation of junction edge effects are the deformations δ (horizontal displacement at any point on the shell, positive when away from the axis of revolution) and V (rotation of the meridian). For axisymmetrically loaded spherical shells, these deformations may be written directly in terms of stress resultants N_ϕ and N_θ as follows [5]:

$$\delta^m = \frac{a}{Et}(\sin\phi)(N_\theta - \nu N_\phi) \quad (27a)$$

$$V^m = \frac{1}{Et}\left\{(1+\nu)(N_\phi - N_\theta)\cot\phi - \frac{d}{d\phi}(N_\theta - \nu N_\phi)\right\} \quad (27b)$$

For the present problem, and considering shell S*i*, the above equations become

$$\delta^m = \frac{\gamma a_i^3}{6Et}(\sin\phi)\left\{6\left(\frac{k_i}{a_i} - \cos\phi\right) - \frac{1+\nu}{\sin^2\phi}\left(2\cos^3\phi - 3\frac{k_i}{a_i}\cos^2\phi + C_i\right)\right\} \quad (28a)$$

$$V^m = -\frac{\gamma a_i^2}{Et}\sin\phi \quad (28b)$$

Let us denote an arbitrary shell junction (J1, J2, J3, etc.) by O. At junction O (see Fig. 3), let us denote the parameters pertaining to the upper shell by plain symbols (without a prime), and parameters pertaining to the lower shell by primed symbols. Thus, at a junction where shell S*i* is connected to shell S$(i+1)$, the angle ϕ_{i2} (corresponding to the lower edge of shell S*i*) becomes simply ϕ_o, while the angle $\phi_{(i+1)1}$ (corresponding to the upper edge of shell S$(i+1)$) becomes simply ϕ_o'. In this notation, the radii of the upper and lower shells become simply a and a', respectively, and so forth. This notation greatly simplifies the writing down of results for the junction effects, since the same set of expressions become applicable for all junctions of the vessel.

For such an arbitrary junction O, the expression for the horizontal resultant of the membrane meridional stress resultants (Eq. (26)) becomes

$$H_o^m = \frac{1}{6}\frac{\gamma a^2}{\sin^2\phi_o}\left(2\cos^3\phi_o - 3\frac{k}{a}\cos^2\phi_o + C\right)\cos\phi_o - \frac{1}{6} \times \frac{\gamma a'^2}{\sin^2\phi_o'}\left(2\cos^3\phi_o' - 3\frac{k'}{a'}\cos^2\phi_o' + C'\right)\cos\phi_o' \quad (29)$$

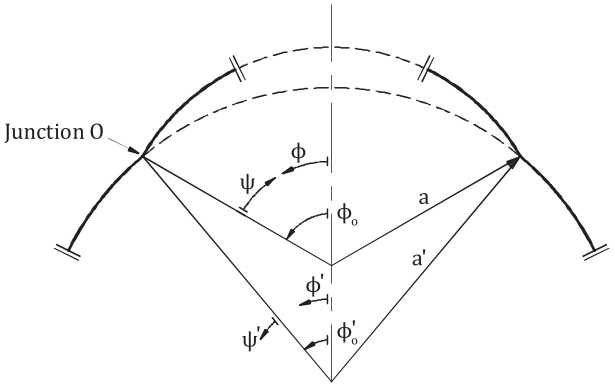

Fig. 3. Arbitrary junction O and geometric parameters for the upper and lower shells.

where the parameters k and C (denoted earlier as k_i and C_i for shell S*i*) relate to the upper shell, and k' and C' relate to the lower shell.

The membrane edge deformations for the upper and lower shells at junction O (refer to Fig. 4(a) for the positive directions of these) become:

$$\delta_o^m = \frac{\gamma a^3}{6Et}(\sin\phi_o)\left\{6\left(\frac{k}{a} - \cos\phi_o\right) - \frac{1+\nu}{\sin^2\phi_o}\left(2\cos^3\phi_o - 3\frac{k}{a}\cos^2\phi_o + C\right)\right\} \quad (30a)$$

$$\delta_o'^m = \frac{\gamma a'^3}{6Et'}(\sin\phi_o')\left\{6\left(\frac{k'}{a'} - \cos\phi_o'\right) - \frac{1+\nu}{\sin^2\phi_o'}\left(2\cos^3\phi_o' - 3\frac{k'}{a'}\cos^2\phi_o' + C'\right)\right\} \quad (30b)$$

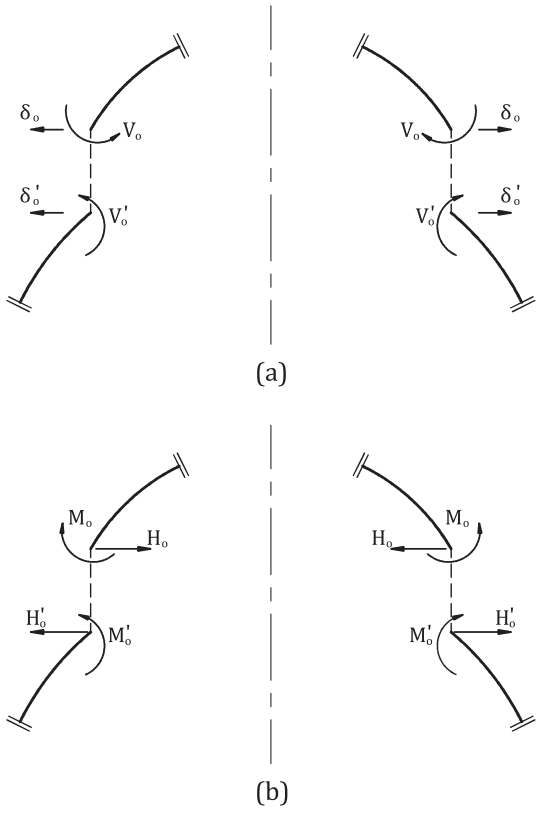

Fig. 4. Edge deformations and axisymmetric edge actions at junction O: (a) horizontal displacements and meridional rotations; (b) horizontal shear forces and bending moments.

$$V_o^m = -\frac{\gamma a^2}{Et}\sin\phi_o \tag{31a}$$

$$V_o'^m = -\frac{\gamma a'^2}{Et'}\sin\phi_o' \tag{31b}$$

where the thickness parameters t and t' refer to the upper and lower shells respectively.

5. Bending solution

Fig. 4(b) shows a system of axisymmetric bending moments and horizontal shearing forces applied at the edges of the upper and lower shells at junction O. Each shell will experience interior bending moments, stress resultants and deformations in the vicinity of the edge (the so-called "edge effect"), in response to the application of these axisymmetric edge actions. To quantify the edge effects, we will adopt the asymptotic solution of Hetényi for the axisymmetric bending of spherical shells [36], which is very accurate provided that the meridional angle of the shell is not too close to zero or 180° (that is, provided ϕ lies in the range $20° \leqslant \phi \leqslant 160°$).

Based on the spherical-shell bending theory of Hetenyi [36], general expressions for interior stress resultants, bending moments and deformations in a spherical shell, due to axisymmetric bending moments and shear forces applied at the edge of the shell, have been developed in reference [5]. We may readily apply the results to the problem depicted in Fig. 4(b).

If the meridional angle measured from the shell edge is denoted by ψ for the upper shell and by ψ' for the lower shell, it is clear, by reference to Fig. 3, that $\psi = \phi_o - \phi$ for the upper shell, and $\psi' = \phi' - \phi_o'$ for the lower shell. Let λ and λ' denote the shell slenderness parameters; for the upper shell, $\lambda = [3(1-\nu^2)(a^2/t^2)]^{1/4}$, and for the lower shell, $\lambda' = [3(1-\nu^2)(a'^2/t'^2)]^{1/4}$.

The results for actions in the interior of the shell and deformations at the shell edge are as follows (the superscript b denotes that these quantities are associated with the bending disturbance).

5.1. Upper shell

$$N_\phi^b = -\cot(\phi_o-\psi)\frac{e^{-\lambda\psi}}{\sqrt{\sin(\phi_o-\psi)}}\left\{\frac{2\lambda}{aK_1}(\sin\phi_o)^{1/2}M_o\sin\lambda\psi - \frac{(1+K_1^2)^{1/2}}{K_1}(\sin\phi_o)^{3/2}H_o\sin(\lambda\psi+\beta)\right\} \tag{32a}$$

$$N_\theta^b = \frac{\lambda}{2}\frac{e^{-\lambda\psi}}{\sqrt{\sin(\phi_o-\psi)}}\left[\frac{2\lambda}{aK_1}(\sin\phi_o)^{1/2}M_o\{2\cos\lambda\psi-(k_1+k_2)\sin\lambda\psi\} - \frac{(1+K_1^2)^{1/2}}{K_1}(\sin\phi_o)^{3/2}H_o\{2\cos(\lambda\psi+\beta)-(k_1+k_2)\sin(\lambda\psi+\beta)\}\right] \tag{32b}$$

$$M_\phi = \frac{a}{2\lambda}\frac{e^{-\lambda\psi}}{\sqrt{\sin(\phi_o-\psi)}}\left[\frac{2\lambda}{aK_1}(\sin\phi_o)^{1/2}M_o\{k_1\cos\lambda\psi+\sin\lambda\psi\} - \frac{(1+K_1^2)^{1/2}}{K_1}(\sin\phi_o)^{3/2}H_o\{k_1\cos(\lambda\psi+\beta)+\sin(\lambda\psi+\beta)\}\right] \tag{33a}$$

$$M_\theta = \frac{a}{4\lambda\nu}\frac{e^{-\lambda\psi}}{\sqrt{\sin(\phi_o-\psi)}}\left[\frac{2\lambda}{aK_1}(\sin\phi_o)^{1/2}M_o \times[\{(1+\nu^2)(k_1+k_2)-2k_2\}\cos\lambda\psi+2\nu^2\sin\lambda\psi] - \frac{(1+K_1^2)^{1/2}}{K_1}(\sin\phi_o)^{3/2}H_o\times[\{(1+\nu^2)(k_1+k_2)-2k_2\}\times\cos(\lambda\psi+\beta)+2\nu^2\sin(\lambda\psi+\beta)]\right] \tag{33b}$$

$$\delta_o^b = \frac{2\lambda^2}{EtK_1}(\sin\phi_o)M_o - \frac{\lambda a}{Et}\left(\frac{1+K_1K_2}{K_1}\right)(\sin^2\phi_o)H_o \tag{34a}$$

$$V_o^b = -\frac{4\lambda^3}{EatK_1}M_o + \frac{2\lambda^2}{EtK_1}(\sin\phi_o)H_o \tag{34b}$$

where

$$k_1 = 1 - \left(\frac{1-2\nu}{2\lambda}\right)\cot(\phi_o-\psi) \tag{35a}$$

$$k_2 = 1 - \left(\frac{1+2\nu}{2\lambda}\right)\cot(\phi_o-\psi) \tag{35b}$$

$$K_1 = 1 - \left(\frac{1-2\nu}{2\lambda}\right)\cot\phi_o \tag{36a}$$

$$K_2 = 1 - \left(\frac{1+2\nu}{2\lambda}\right)\cot\phi_o \tag{36b}$$

$$\beta = -\tan^{-1}(K_1) \tag{37}$$

5.2. Lower shell

$$N_\phi'^b = -\cot(\phi_o'+\psi')\frac{e^{-\lambda'\psi'}}{\sqrt{\sin(\phi_o'+\psi')}}\left\{\frac{2\lambda'}{a'K_1'}(\sin\phi_o')^{1/2}M_o'\sin\lambda'\psi' + \frac{(1+K_1'^2)^{1/2}}{K_1'}(\sin\phi_o')^{3/2}H_o'\sin(\lambda'\psi'+\beta')\right\} \tag{38a}$$

$$N_\theta'^b = \frac{\lambda'}{2}\frac{e^{-\lambda'\psi'}}{\sqrt{\sin(\phi_o'+\psi')}}\left[\frac{2\lambda'}{a'K_1'}(\sin\phi_o')^{1/2}M_o'\{2\cos\lambda'\psi'-(k_1'+k_2')\sin\lambda'\psi'\} + \frac{(1+K_1'^2)^{1/2}}{K_1'}(\sin\phi_o')^{3/2}H_o'\{2\cos(\lambda'\psi'+\beta')-(k_1'+k_2')\sin(\lambda'\psi'+\beta')\}\right] \tag{38b}$$

$$M_\phi' = \frac{a'}{2\lambda'}\frac{e^{-\lambda'\psi'}}{\sqrt{\sin(\phi_o'+\psi')}}\left[\frac{2\lambda'}{a'K_1'}(\sin\phi_o')^{1/2}M_o'\{k_1'\cos\lambda'\psi'+\sin\lambda'\psi'\} + \frac{(1+K_1'^2)^{1/2}}{K_1'}(\sin\phi_o')^{3/2}H_o'\{k_1'\cos(\lambda'\psi'+\beta')+\sin(\lambda'\psi'+\beta')\}\right] \tag{39a}$$

$$M_\theta' = \frac{a'}{4\lambda'\nu}\frac{e^{-\lambda'\psi'}}{\sqrt{\sin(\phi_o'+\psi')}}\left[\frac{2\lambda'}{a'K_1'}(\sin\phi_o')^{1/2}M_o'\times[\{(1+\nu^2)(k_1'+k_2') - 2k_2'\}\cos\lambda'\psi'+2\nu^2\sin\lambda'\psi'] + \frac{(1+K_1'^2)^{1/2}}{K_1'}(\sin\phi_o')^{3/2}H_o' \times[\{(1+\nu^2)(k_1'+k_2')-2k_2'\}\cos(\lambda'\psi'+\beta')+2\nu^2\sin(\lambda'\psi'+\beta')]\right] \tag{39b}$$

$$\delta_o'^b = \frac{2\lambda'^2}{Et'K_1'}(\sin\phi_o')M_o' + \frac{\lambda' a'}{Et'}\left(\frac{1+K_1'K_2'}{K_1'}\right)(\sin^2\phi_o')H_o' \tag{40a}$$

$$V_o'^b = \frac{4\lambda'^3}{Ea't'K_1'}M_o' + \frac{2\lambda'^2}{Et'K_1'}(\sin\phi_o')H_o' \tag{40b}$$

where

$$k_1' = 1 + \left(\frac{1-2\nu}{2\lambda'}\right)\cot(\phi_o'+\psi') \tag{41a}$$

$$k_2' = 1 + \left(\frac{1+2\nu}{2\lambda'}\right)\cot(\phi_o'+\psi') \tag{41b}$$

$$K_1' = 1 + \left(\frac{1-2\nu}{2\lambda'}\right)\cot\phi_o' \tag{42a}$$

$$K_2' = 1 + \left(\frac{1+2\nu}{2\lambda'}\right)\cot\phi_o' \tag{42b}$$

$$\beta' = -\tan^{-1}(K_1') \tag{43}$$

6. Evaluation of edge actions

To evaluate the edge actions M_o, H_o, M_o', H_o', we apply the boundary conditions of continuity of net deformations across the junction of the two shells

$$\delta_o^T = \delta_o'^T \tag{44a}$$

$$V_o^T = V_o'^T \tag{44b}$$

and the boundary conditions expressing the equilibrium of an element at the interface of the two shells, namely that the net torque and the net horizontal thrust upon such an element must be zero:

$$M_o - M_o' = 0 \tag{45a}$$

$$H_o^m + H_o' - H_o = 0 \tag{45b}$$

Net deformations $\delta_o^T, \delta_o'^T, V_o^T, V_o'^T$ are, of course, given by superimposing the components due to the bending correction – expressions (34) and (40) – with their membrane-solution counterparts. The latter have already been obtained explicitly (results (30) and (31)), and may therefore be taken as known quantities. Thus

$$\delta_o^T = \delta_o^m + \frac{2\lambda^2}{EtK_1}(\sin\phi_o)M_o - \frac{\lambda a}{Et}\left(\frac{1+K_1K_2}{K_1}\right)(\sin^2\phi_o)H_o \tag{46a}$$

$$\delta_o'^T = \delta_o'^m + \frac{2\lambda'^2}{Et'K_1'}(\sin\phi_o')M_o' + \frac{\lambda' a'}{Et'}\left(\frac{1+K_1'K_2'}{K_1'}\right)\left(\sin^2\phi_o'\right)H_o' \tag{46b}$$

$$V_o^T = V_o^m - \frac{4\lambda^3}{EatK_1}M_o + \frac{2\lambda^2}{EtK_1}(\sin\phi_o)H_o \tag{47a}$$

$$V_o'^T = V_o'^m + \frac{4\lambda'^3}{Ea't'K_1'}M_o' + \frac{2\lambda'^2}{Et'K_1'}(\sin\phi_o')H_o' \tag{47b}$$

From Eq. (45), we obtain the relations

$$M_o' = M_o \tag{48a}$$

$$H_o' = H_o - H_o^m \tag{48b}$$

where H_o^m is a known quantity (result (29)). Using relations (46) and (47) to write out Eqs. (44) in expanded form, and eliminating M_o' and H_o' from the ensuing pair of equations (using relations (48)), we obtain a pair of simultaneous equations in two unknowns M_o and H_o, which upon solving yield

$$M_o = \frac{f_1 g_1 - f_2 g_2}{f_1^2 - f_2 f_3} \tag{49a}$$

$$H_o = \frac{f_1 g_2 - f_3 g_1}{f_1^2 - f_2 f_3} \tag{49b}$$

where

$$f_1 = \frac{2}{E}\left\{\frac{\lambda^2}{tK_1}(\sin\phi_o) - \frac{\lambda'^2}{t'K_1'}(\sin\phi_o')\right\} \tag{50a}$$

$$f_2 = -\frac{1}{E}\left\{\frac{\lambda a}{t}\left(\frac{1+K_1K_2}{K_1}\right)(\sin^2\phi_o) + \frac{\lambda' a'}{t'}\left(\frac{1+K_1'K_2'}{K_1'}\right)(\sin^2\phi_o')\right\} \tag{50b}$$

$$f_3 = -\frac{4}{E}\left(\frac{\lambda^3}{atK_1} + \frac{\lambda'^3}{a't'K_1'}\right) \tag{50c}$$

$$g_1 = (\delta_o')^m - (\delta_o)^m - \frac{\lambda' a'}{Et'}\left(\frac{1+K_1'K_2'}{K_1'}\right)\left(\sin^2\phi_o'\right)H_o^m \tag{50d}$$

$$g_2 = (V_o')^m - (V_o)^m - \frac{2\lambda'^2}{Et'K_1'}(\sin\phi_o')H_o^m \tag{50e}$$

The other two edge actions M_o' and H_o' then follow from relations (48).

7. Net stresses

With the shell-edge actions $\{M_o, H_o, M_o', H_o'\}$ now known, we can evaluate, from expressions (32), (33), (38) and (39), the bending-related stress resultants $\{N_\phi^b, N_\theta^b, N_\phi'^b, N_\theta'^b\}$ and bending moments $\{M_\phi, M_\theta, M_\phi', M_\theta'\}$ in the two shells. The net stresses on the inner and outer surfaces of the two shells then follow by superimposing the membrane-solution stresses with those stemming from the bending correction:

$$\sigma_\phi^T = \frac{N_\phi^m}{t} + \frac{N_\phi^b}{t} \pm \frac{6M_\phi}{t^2} \tag{51a}$$

$$\sigma_\theta^T = \frac{N_\theta^m}{t} + \frac{N_\theta^b}{t} \pm \frac{6M_\theta}{t^2} \tag{51b}$$

$$\sigma_\phi'^T = \frac{N_\phi'^m}{t'} + \frac{N_\phi'^b}{t'} \pm \frac{6M_\phi'}{t'^2} \tag{52a}$$

$$\sigma_\theta'^T = \frac{N_\theta'^m}{t'} + \frac{N_\theta'^b}{t'} \pm \frac{6M_\theta'}{t'^2} \tag{52b}$$

8. Numerical example

Fig. 5 shows a vessel consisting of three shells of radii $a_1 = 10$ m (shell A), $a_2 = 13.473$ m (shell B) and $a_3 = 10$ m (shell C). These meet at junctions J1 and J2 as shown. In the notation of the present formulation, the shells A, B, C will be denoted by S1, S2, S3 respectively. The uppermost shell (shell S1) has an angle of opening $\phi_{10} = 60^\circ$; the bottom shell (shell S3) has an angle of opening $\phi_{30} = 120^\circ$; the middle shell (shell S2) has angles of opening $\phi_{21} = 40^\circ$ at junction J1 and $\phi_{22} = 140^\circ$ at junction J2. The shells are assumed to be fabricated from steel plate of constant thickness $t = 0.05$ m throughout, giving a minimum radius-to-thickness ratio of 200 for the vessel. The Young modulus of steel will be taken as $E = 200 \times 10^9$ N/m^2, and the Poisson ratio of steel as $\nu = 0.3$.

The geometrical configuration of the whole assembly is symmetrical about the equatorial (middle) plane of the vessel. The vessel is assumed to be axisymmetrically supported in the lower region of shell S3, the distance of the supports (from junction J2) being such that the edge effects at the supports do not significantly influence the edge effects at junction J2 (which is valid if the location of the supports is below the level $\phi = 150^\circ$). It is assumed that the vessel is completely filled with water of unit weight $\gamma = 10 \times 10^3$ N/m^3. A brief summary of the correct sequence of calculations is as follows:

First, we calculate the depth parameters h_{10} and h_{22} using Eqs. (2b) and (3b) respectively, then the parameters k_1, k_2 and k_3 for the three shells using Eqs. (7a), (7b) and (7d) respectively. The constant of integration of the membrane solution for the top cap (shell S1) is $C_1 = 1$. The constants of integration C_2 and C_3 (for shells S2 and S3 respectively) are evaluated from Eqs. (20) and (24) using

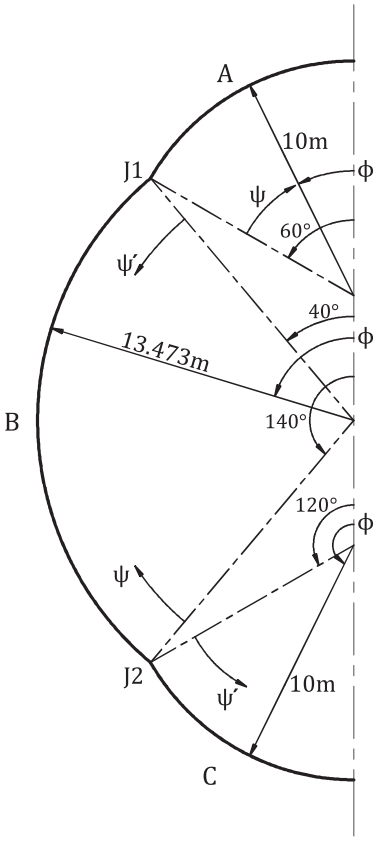

Fig. 5. Geometric parameters of the numerical example.

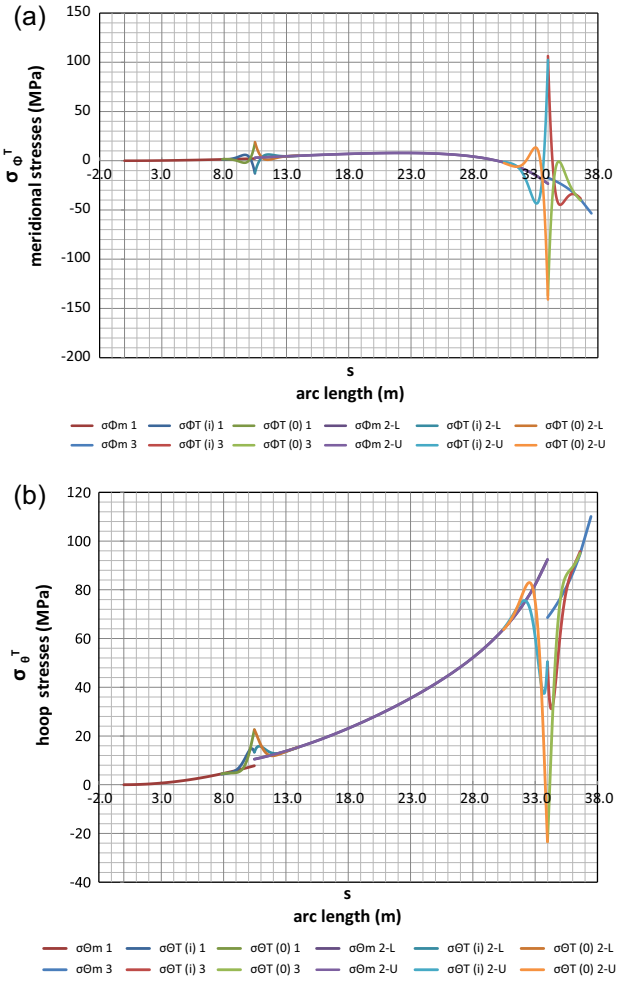

Fig. 6. Variations of stresses with arc length s over the full profile of the vessel (top to bottom): (a) meridional stresses; (b) hoop stresses. In the legend, the symbol m denotes membrane stresses, $T(i)$ denotes total stresses on the inner surface of the shell, and $T(o)$ denotes total stresses on the outer surface of the shell.

the relevant geometric parameters. The variations of membrane stress resultants in shells S1, S2 and S3 then follow from Eqs. (13), (21) and (25). We then use Eq. (29) to evaluate the horizontal resultant of the membrane meridional stress resultants at the junctions, and Eqs. (30) and (31) to evaluate the membrane deformations at the junctions. That finishes the calculation of all relevant membrane quantities.

The quantities associated with the bending effects are evaluated next. Knowing the slenderness parameter λ for each of the three shells, we evaluate the bending-solution parameters represented by Eqs. (35)–(37) for the upper side of a given junction, and Eqs. (41)–(43) for the lower side of a given junction. The parameters $\{f_1, f_2, f_3, g_1, g_2\}$ are evaluated from Eqs. (50); the actions $\{M_o, H_o\}$ at the upper edge of a given junction follow from Eqs. (49), while the actions $\{M'_o, H'_o\}$ at the lower edge of a given junction follow from Eqs. (48). Using these values of $\{M_o, H_o, M'_o, H'_o\}$, the bending-related stress resultants $\{N^b_\phi, N^b_\theta, N'^b_\phi, N'^b_\theta\}$ and bending moments $\{M_\phi, M_\theta, M'_\phi, M'_\theta\}$ in the junction zones are evaluated on the basis of Eqs. (32), (33), (38) and (39). Combining the membrane stresses with the bending-related stresses in accordance with Eqs. (51) and (52) then gives the final stresses in the shell.

A finite-element analysis of the vessel was performed using the programme ABAQUS [37]. Three-node curved-line (quadratic) axisymmetric shell elements with two integration points (SAX2) were used for the modelling of the entire vessel. The mesh was made very fine in the neighbourhood of the junctions (3 m on either side to cover the effective range of the bending disturbance), with each element subtending an angle of 0.1°. This fine mesh was also used throughout the lower part of the vessel below junction J2, in order to properly account for support-related bending effects. Outside the bending-disturbance zones, a coarser mesh (elements subtending an angle of 1.0°) was found to suffice.

Axisymmetric support conditions (with all three degrees of freedom fixed) were prescribed at the location $\phi_s = 150°$ of shell C, sufficiently distanced from junction J2 ($\phi_{30} = 120°$) to ensure that edge-disturbance interaction [38] between the supports and junction J2 was insignificant. Hydrostatic pressure normal to the shell inner surface was applied. Output results were obtained in the form of stress components S11 (meridional) and S22 (hoop) calculated at the integration points of each element.

9. Results and discussion

Fig. 6(a) and (b) shows meridional and hoop stresses (in MPa), respectively, plotted versus the coordinate s, this being the *cumulative* distance travelled from the apex of the vessel along the curved meridian, up to the point in question. For points lying on shell A, this distance is simply the arc length over shell A up to the point in question; for points lying on shell B, it will be the full arc length of shell A, plus the additional arc length from junction J1 over shell B up to the point in question; for points lying on shell C, the distance s will be the sum of the full arc lengths of shells A and B, plus the additional arc length from junction J2 over shell C up to the point in question. The range of s covered by the plots is $0 \leqslant s \leqslant 37.5$ m.

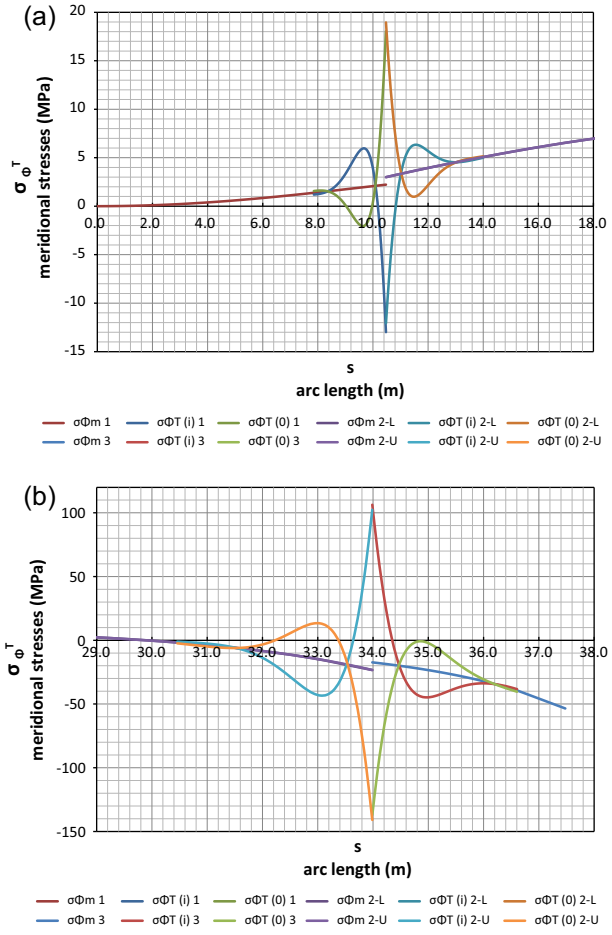

Fig. 7. Meridional stress variations in the vicinity of the shell junctions: (a) junction J1; (b) junction J2. In the legend, the symbol m denotes membrane stresses, $T(i)$ denotes total stresses on the inner surface of the shell, and $T(o)$ denotes total stresses on the outer surface of the shell.

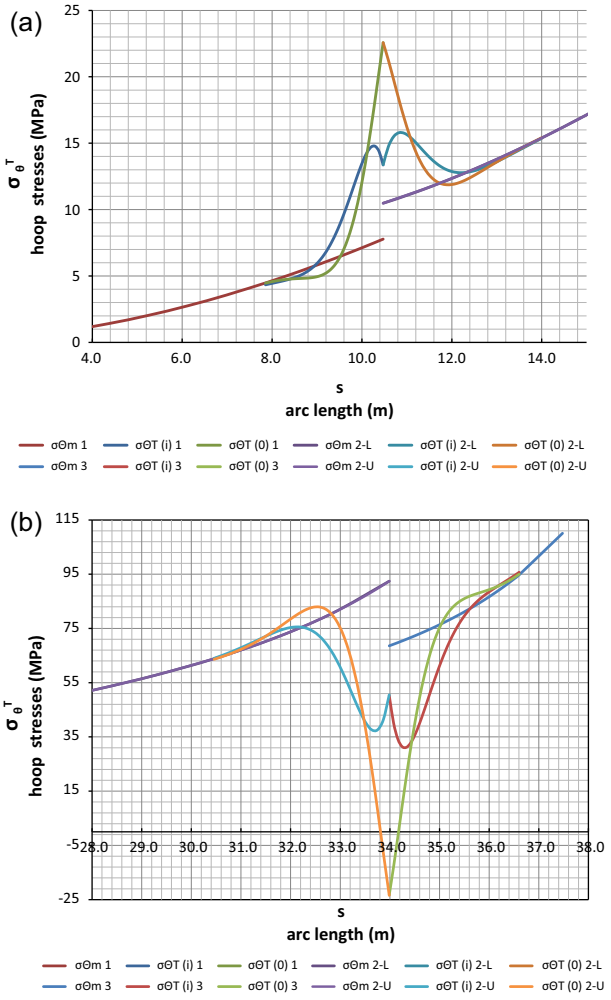

Fig. 8. Hoop stress variations in the vicinity of the shell junctions: (a) junction J1; (b) junction J2. In the legend, the symbol m denotes membrane stresses, $T(i)$ denotes total stresses on the inner surface of the shell, and $T(o)$ denotes total stresses on the outer surface of the shell.

In these plots, the gradually varying curves are the membrane stresses $\{\sigma_\phi^m, \sigma_\theta^m\}$, while the sharply oscillating curves in the vicinity of the junction locations represent total stresses on the inner and outer shell surfaces, that is $\{\sigma_\phi^T(i); \sigma_\phi^T(o)\}$ for the meridional-stress variations in Fig. 6(a), and $\{\sigma_\theta^T(i); \sigma_\theta^T(o)\}$ for the hoop-stress variations in Fig. 6(b). Some observations are as follows:

(i) As expected, the membrane-stress variations show discontinuities (or jumps) at both junctions J1 and J2. On combining the membrane stresses with the stresses due to the edge effect, the total-stress variations show continuity in values (but not of slope) across the junctions.

(ii) The bending-disturbance stresses at the lower junction are several times larger than those at the upper junction; this is because the larger hydrostatic pressures in the lower part of the vessel cause bigger membrane-deformation incompatibilities, in turn inducing larger bending effects.

(iii) The bending-disturbance stresses are very localised to the shell junctions, dying out within a distance of only 2.5 m on either side of the junctions. However, within these narrow zones, they sharply rise to magnitudes that are several times larger than the calculated membrane stresses.

(iv) At both the upper and the lower junctions, the bending-disturbance effects result in net meridional stresses in both tension and compression that are relatively large in comparison with the surrounding membrane stresses.

Table 1
Meridional stress values (in MPa) at the junction locations.

	Junction J1			Junction J2		
	σ_ϕ^m	σ_ϕ^T (outer)	σ_ϕ^T (inner)	σ_ϕ^m	σ_ϕ^T (outer)	σ_ϕ^T (inner)
Upper side	2.2	18.0	−13.0	−23.3	−141.0	102.4
Lower side	3.0	19.0	−12.1	−17.3	−137.1	106.3

Table 2
Hoop stress values (in MPa) at the junction locations.

	Junction J1			Junction J2		
	σ_θ^m	σ_θ^T (outer)	σ_θ^T (inner)	σ_θ^m	σ_θ^T (outer)	σ_θ^T (inner)
Upper side	7.8	22.6	13.4	92.4	−23.4	50.5
Lower side	10.5	22.6	13.4	68.6	−23.3	50.3

(v) On the other hand, while the bending disturbance increases the relatively modest membrane hoop tension at the upper junction, it has the beneficial effect of sharply lowering the

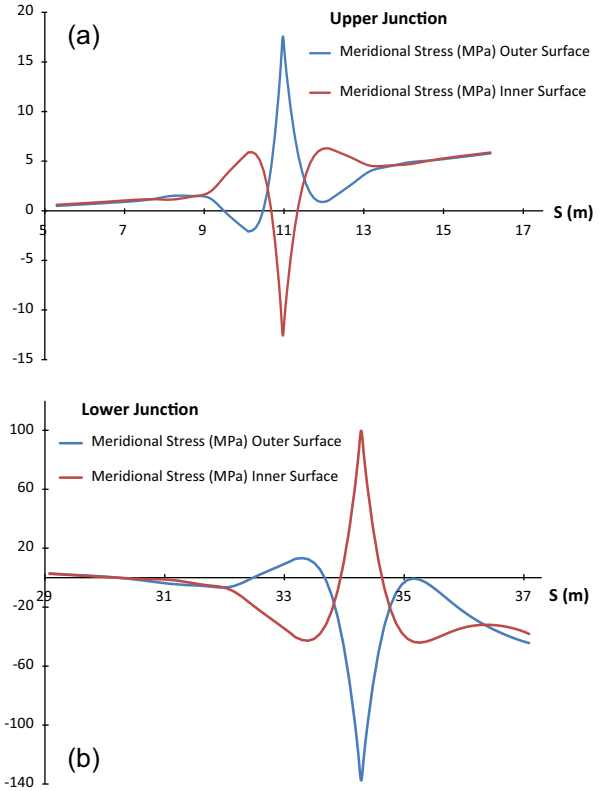

Fig. 9. FEM results: meridional stress variations in the vicinity of the shell junctions: (a) junction J1; (b) junction J2.

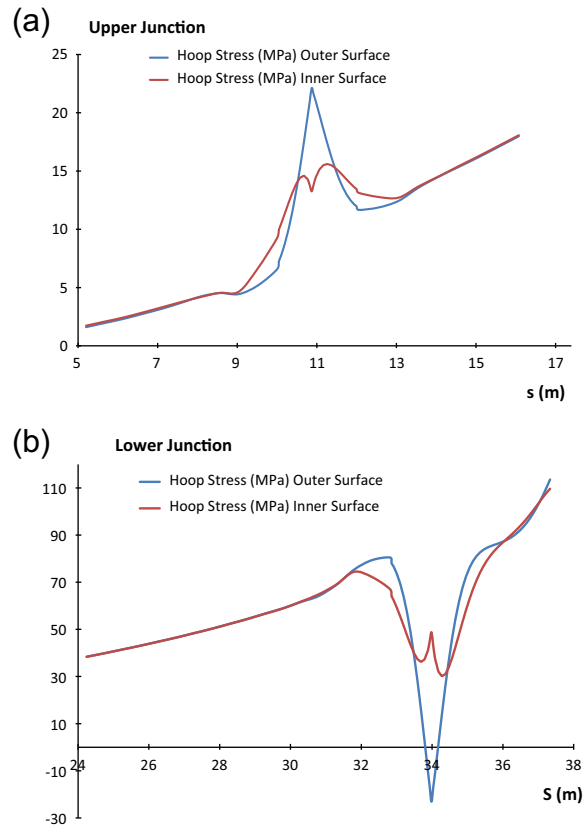

Fig. 10. FEM results: hoop stress variations in the vicinity of the shell junctions: (a) junction J1; (b) junction J2.

Table 3
Analytical versus FEM results for junction locations (values in MPa).

	Junction J1				Junction J2			
	$\sigma_\phi^T\ (o)$	$\sigma_\phi^T\ (i)$	$\sigma_\theta^T\ (o)$	$\sigma_\theta^T\ (i)$	$\sigma_\phi^T\ (o)$	$\sigma_\phi^T\ (i)$	$\sigma_\theta^T\ (o)$	$\sigma_\theta^T\ (i)$
ANA	18.5	−12.6	22.6	13.4	−139.1	104.4	−23.4	50.4
FEM	17.6	−12.6	22.1	13.3	−137.5	99.7	−23.1	49.5

much larger membrane hoop tension at the lower junction, with the result that outer parts of the shell end up being slightly in compression.

(vi) The inward-pointing kink in the vessel profile at junction J2 has the same effect as circumferentially prestressing the smooth shell at this level (in order to counter hoop tension due to outward hydrostatic pressure). However, the benefit is only very localised.

To see more clearly what is happening in the vicinity of the junctions, the meridional stress variations around junction J1 have been magnified in Fig. 7(a), while those around junction J2 have been magnified in Fig. 7(b). Similarly, Fig. 8(a) shows magnified hoop-stress variations around junction J1, while Fig. 8(b) shows magnified hoop-stress variations around junction J2. Tables 1 and 2 feature meridional and hoop stress values (in N/mm^2) at junctions J1 and J2, for the upper and lower sides of the junctions.

The results of the finite-element analysis are plotted in Figs. 9 and 10. Comparing Fig. 7(a) versus 9(a), 7(b) versus 9(b), 8(a) versus 10(a), and 8(b) versus 10(b), we can see that the agreement between analytical and FEM stress variations is excellent. Table 3 compares analytical and FEM stress values at the junction locations, with the analytical values being the average of the values on either side of the junction. The agreement is very close (generally within 2%), showing that the theoretical formulation developed in this paper is very accurate.

10. Concluding remarks

A theoretical formulation for the complete determination of the state of stress in large thin-walled liquid-filled vessels in the form of multi-segmented spherical shells has been presented. The formulation assumes that the transfer of membrane forces between adjacent shell segments is such that only vertical equilibrium of stress resultants needs to be preserved. The edge effect in the vicinity of the shell junctions is accounted for by an axisymmetric bending theory for spherical shells.

The formulation has been applied to the example of a large 3-segmented vessel, and the results compared to those obtained from finite-element modelling. Excellent agreement between the theoretical and FEM results has been obtained, showing that the presented theoretical formulation is reliable and very accurate. The analytical formulation (which may easily be programmed) may be used to perform rigorous stress analyses of multi-segmented spherical vessels in lieu of finite-element modelling, or to validate new finite-element programmes.

Acknowledgements

The authors would like to thank Mr. Angus Rule of the University of Cape Town for assistance with the preparation of the illustrations. The first author acknowledges funding received from the National Research Foundation of South Africa for the purposes of this research.

References

[1] Tooth AS. Storage vessels. Developments in thin-walled structures, vol. 1. London: Elsevier Applied Science; 1982. p. 1–52.
[2] Novozhilov VV. Thin shell theory. Groningen: Wolters-Noordhoff; 1970.
[3] Flugge W. Stresses in shells. Berlin: Springer-Verlag; 1973.
[4] Gould PL. Analysis of shells and plates. New York: Springer-Verlag; 1988.
[5] Zingoni A. Shell structures in civil and mechanical engineering. London: Thomas Telford; 1997.
[6] Bathe KJ. Finite element procedures in engineering analysis. Englewood Cliffs (NJ): Prentice-Hall; 1982.
[7] Gould PL. Finite element analysis of shells of revolution. Pitman Publishing; 1985.
[8] Chapelle D, Bathe KJ. The finite element analysis of shells: fundamentals. 2nd ed. New York: Springer; 2011.
[9] Zingoni A. On membrane solutions for elevated shell-of-revolution tanks of certain meridional profiles. Thin-Wall Struct 1995;22:121–42.
[10] Zingoni A. Stress analysis of a storage vessel in the form of a complete triaxial ellipsoid: hydrostatic effects. Int J Pressure Vessels Piping 1995;62:269–79.
[11] Chen L, Rotter JM, Doerich C. Buckling of cylindrical shells with stepwise variable wall thickness under uniform external pressure. Eng Struct 2011;33:3570–8.
[12] Zingoni A, Pavlovic MN. Discontinuity phenomena around the supports of stepwise-thickened spherical steel tanks: theoretical considerations and parametric results. Int J Pressure Vessels Piping 1993;53:405–35.
[13] Sosa EM, Godoy LA. Challenges in the computation of lower-bound buckling loads for tanks under wind pressures. Thin-Wall Struct 2010;48:935–45.
[14] Zhao Y, Lin Y. Buckling of cylindrical open-topped steel tanks under wind load. Thin-Wall Struct 2014;79:83–94.
[15] Burgos CA, Jaca RC, Lassig JL, Godoy LA. Wind buckling of tanks with conical roof considering shielding by another tank. Thin-Wall Struct 2014;84:226–40.
[16] Zhao Y, Lin Y, Shen YB. Wind loads on large cylindrical open-topped tanks in group. Thin-Wall Struct 2014;78:108–20.
[17] Shekari MR, Khaji N, Ahmadi MT. On the seismic behavior of cylindrical base-isolated liquid storage tanks excited by long-period ground motions. Soil Dyn Earthquake Eng 2010;30:968–80.
[18] Ozdemir Z, Souli M, Fahjan YM. Application of nonlinear fluid–structure interaction methods to seismic analysis of anchored and unanchored tanks. Eng Struct 2010;32:409–23.
[19] Taniguchi T, Ando Y, Nakashima T. Fluid pressure on unanchored rigid flat-bottom cylindrical tanks due to uplift motion and its approximation. Eng Struct 2009;31:2598–606.
[20] Guggenberger W. Collapse design of large steel digester tanks. Thin-Wall Struct 1994;20:109–28.
[21] Rotter JM. Shell structures: the new European standard and current research needs. Thin-Wall Struct 1998;31:3–23.
[22] Rotter JM. Recent advances in the philosophy of the practical design of shell structures, implemented in Eurocode provisions. In: Zingoni A, editor. Recent developments in structural engineering, mechanics and computation. Rotterdam: Millpress; 2007. p. 26–31.
[23] Zingoni A. Stresses and deformations in egg-shaped sludge digesters: membrane effects. Eng Struct 2001;23:1365–72.
[24] Zingoni A. Stresses and deformations in egg-shaped sludge digesters: discontinuity effects. Eng Struct 2001;23:1373–82.
[25] Zingoni A. Parametric stress distribution in shell-of-revolution sludge digesters of parabolic ogival form. Thin-Wall Struct 2002;40:691–702.
[26] El Damatty AA, Marroquin EG, El Attar M. Behavior of stiffened liquid-filled conical tanks. Thin-Wall Struct 2001;39:353–73.
[27] El Damatty AA, Marroquin E. Design procedure for stiffened water-filled steel conical tanks. Thin-Wall Struct 2002;40:263–82.
[28] Zingoni A. Discontinuity effects at cone–cone axisymmetric shell junctions. Thin-Wall Struct 2002;40:877–91.
[29] Zingoni A. Simplification of the derivation of influence coefficients for symmetric frusta of shells of revolution. Thin-Wall Struct 2009;47:912–8.
[30] Golzan BS, Showkati H. Buckling of thin-walled conical shells under uniform external pressure. Thin-Wall Struct 2008;46:516–29.
[31] Hafeez G, El Ansary AM, El Damatty AA. Stability of combined imperfect conical tanks under hydrostatic loading. J Constr Steel Res 2010;66:1387–97.
[32] Sweedan AMI, El Damatty AA. Simplified procedure for design of liquid-storage combined conical tanks. Thin-Wall Struct 2009;47:750–9.
[33] Jasion P, Magnucki K. Elastic buckling of horizontal barrelled shells filled with liquid: numerical analysis. Thin-Wall Struct 2012;52:117–25.
[34] Zhan HJ, Redekop D. Static and dynamic loading of an ovaloid toroidal tank. Thin-Wall Struct 2009;47:760–7.
[35] Teng JG. Buckling of thin shells: recent advances and trends. Appl Mech Rev (Trans ASME) 1996;49:263–74.
[36] Hetenyi M. Beams on elastic foundation. Ann Arbor: University of Michigan Press; 1946.
[37] ABAQUS Standard. Newark (California): Hibbit, Karlsson and Sorenson Inc: 1998.
[38] Zingoni A, Pavlovic MN. On edge-disturbance interaction and decoupling errors in thin-walled nonshallow spherical-shell frusta. Thin-Wall Struct 1992;13:375–86.